Quenching of I($^2P_{1/2}$) by Cl_2 and Cl Atoms over the Temperature Range 297−663 K†

Anatoly V. Komissarov and Michael C. Heaven*

Department of Chemistry, Emory University, Atlanta, Georgia 30322

Received: March 4, 2003; In Final Form: May 30, 2003

Time-resolved fluorescence measurements have been used to examine the quenching of I($^2P_{1/2}$) by Cl_2 and Cl atoms. Pulsed photolysis of CF_3I was used to generate I*. Quenching by Cl_2 was examined using 248 nm photolysis as Cl_2 does not absorb significantly at this wavelength. Photolysis at 308 nm, which dissociates both CF_3I and Cl_2, was used to investigate quenching by Cl atoms. Quenching kinetics were characterized over the temperature range from 297 to 663 K. The rate constant for quenching by Cl atoms was found to be almost independent of temperature, whereas the rate constant for Cl_2 increased by 3 orders of magnitude in going from 297 to 663 K. Theoretical calculations show that quenching by Cl atoms is mediated by a curve crossing process. The temperature dependence of the Cl_2 quenching rate constant is attributed to the reactive channel I* + Cl_2 → ICl + Cl(^{2}P).

Introduction

Physical and chemical quenching of I($^2P_{1/2}$) (═I*) by Cl atoms and Cl_2 molecules are processes that are of importance in chemically driven oxygen iodine lasers.[1] As a consequence, the room-temperature quenching rate constants were investigated more than 20 years ago.[2−7] The recent development of a chemical iodine laser that is driven by energy transfer from the NCl($a^1\Delta$) radical (the all gas-phase iodine laser or AGIL)[8,9] has now stimulated interest in the temperature dependencies of the I* quenching rate constants. Cl atoms are used in AGIL to generate NCl(a) and they are formed by the NCl(X) self-reaction[10]

$$NCl(X) + NCl(X) \rightarrow N_2 + 2Cl$$

Cl_2 molecules may be generated by the subsequent recombination reaction. As the chemistry used to generate NCl(a) involves several exothermic steps, and energy transfer from NCl(a) to I is significantly exothermic, the subsonic version of the laser operates at relatively high temperatures (500−700 K). Hence, the temperature dependencies of the I* + Cl and I* + Cl_2 quenching rate constants must be known to permit analysis of device performance and the prediction of conditions that would yield the optimum efficiency.

Quenching of I* by Cl is also of interest from a theoretical perspective. It is most likely that the mechanism by which this process occurs involves crossings of the ICl potential energy curves that correlate with the I*+Cl and I+Cl(^{2}P) dissociation asymptotes[5] (here we use Cl(^{2}P) to indicate atoms that may be in either the $J = 3/2$ or $J = 1/2$ states). These curve crossings have been probed in studies of ICl photodissociation dynamics[11−13] and their characteristics have been predicted using high-level electronic structure calculations.[14] Hence it is of interest to see if the information derived from spectroscopic and theoretical studies of ICl can provide a quantitative description of I* + Cl quenching.

Room-temperature studies of I* + Cl quenching show that this is a very facile process. Burrows[4] and De Juan and Smith[5] reported rate constants of 1.5×10^{-11} and $(2\pm1) \times 10^{-11}$ cm^3 s^{-1}, respectively. Hall et al.[6] estimated that the rate constant could be as high as 2×10^{-10} cm^3 s^{-1}, but the lower values are generally accepted. In contrast, room-temperature quenching of I* by Cl_2 is slow to the point where it is difficult to determine the rate constant[4,6,7]. Early measurements[3,2] that involved photolytic generation of I* in the presence of Cl_2 were complicated by co-photolysis of Cl_2, followed by rapid I* + Cl quenching. Burrows [4] and Hall et al.[6] made careful studies of this problem using pulsed laser photolysis of CF_3I (or C_3F_7I)/Cl_2 mixtures. Burrows[4] obtained a Cl_2 quenching rate constant of $(2.0\pm0.1) \times 10^{-14}$, whereas Hall et al.[6] gave an upper bound of $<8 \times 10^{-15}$ cm^3 s^{-1}. Discharge flow methods were also used to examine I* + Cl_2. De Juan and Smith[5] obtained an upper bound for the quenching rate constant of $<5 \times 10^{-14}$, and Lilenfeld et al.[7] reported $(1.7\pm0.7) \times 10^{-14}$ cm^3 s^{-1}. ICl is an efficient quencher of I* ($k = 2 \times 10^{-11}$ cm^3 s^{-1}),[4,7] so the presence of small concentrations of ICl was an additional complication for both the photolysis and discharge flow experiments. In the analysis of the former, it was suggested[6] that some ICl originated from a slow pre-reaction between CF_3I and Cl_2. Secondary photochemical reactions contributed a much faster time dependent component to the ICl concentration.

In the present study, we have examined the I* + Cl and I* + Cl_2 quenching rate constants over the temperature range from 297 to 663 K. We find that quenching by Cl atoms is almost temperature independent over the range examined. A theoretical model for the quenching of I* by Cl has been examined, using curve crossing information derived from recent electronic structure calculations for ICl. The results are in good agreement with the experimental observations, indicating that a specific avoided crossing between a pair of 0^+ curves is responsible for the efficient quenching process. In contrast to the I* + Cl system, the rate constant for removal of I* by Cl_2 increases rapidly with increasing temperature. Our measurements do not show if the enhancement of the quenching process comes from physical or chemical interactions, but we speculate that a modest

† Part of the special issue "Charles S. Parmenter Festschrift".

* To whom correspondence should be addressed. Phone: 404 727 6617. Fax: 404 727 6586. E-mail: heaven@euch4e.chem.emory.edu.

10.1021/jp034556v CCC: $25.00
Published on Web 07/19/2003

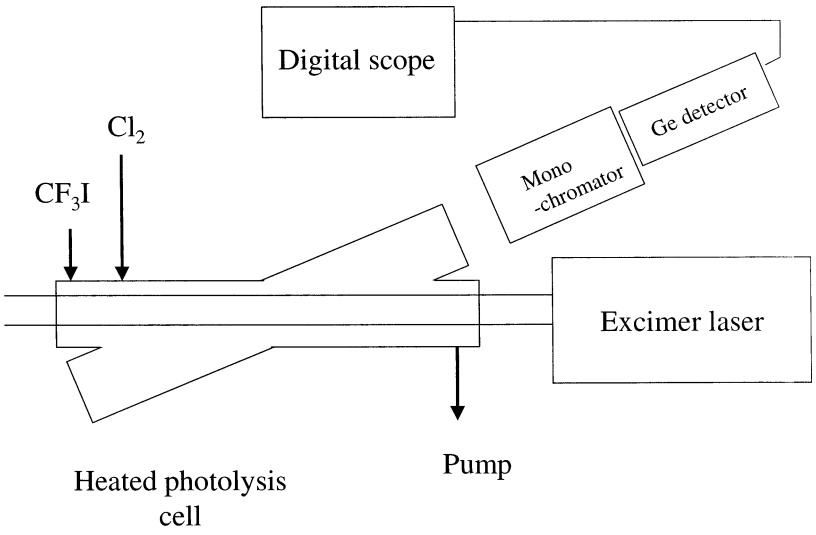

Figure 1. Apparatus used to investigate quenching of I* by Cl_2 and Cl. The photolysis cell was wrapped with heating tape and insulation (not shown).

barrier in the I* + Cl_2 → ICl + Cl(^{2}P) reaction path is the primary cause of the observed behavior.

Experimental Section

A schematic diagram of the apparatus used for these experiments is shown in Figure 1. The photolysis cell consisted of a 5 cm diameter glass cell of 35 cm length. The cell was equipped with quartz windows for transmission of the photolysis beam and a capacitance manometer for pressure measurements (MKS 390HA-00100). For fluorescence observation, a second set of windows was mounted along an axis that was rotated approximately 30° from the photolysis beam axis. The entire body of the cell was wrapped in heating tape with an outer layer of fiberglass insulation (not shown in Figure 1). The temperature in the center of the cell was measured by a thin wire type K thermocouple. Stable temperatures of up to 700 K could be sustained in this apparatus.

Measurements were made under slow flow conditions. CF_3I was mixed with He buffer gas before entering the photolysis cell. Using an He flow rate of approximately 500 sccm, the vacuum pump was throttled to give total cell pressures in the range of 9−10 Torr. The flow of CF_3I, controlled using a needle valve, was adjusted to give a partial pressure in the cell of 0.5 Torr. A flow of pure Cl_2, also controlled by a needle valve, was added to the cell. The flow was adjusted to give Cl_2 partial pressures in the range of 0−0.7 Torr. It was assumed that the Cl_2 partial pressure was equal to the increase in the cell pressure observed when the Cl_2 flow was established.

CF_3I and CF_3I/Cl_2 mixtures were photolyzed by 10 ns pulses from excimer lasers (Questek 2000 for 248 nm and Lambda Physik Lextra for 308 nm). For most measurements, the lasers were operated at a repetition rate of 0.5 Hz with intensities in the range of 20−50 (248) and 100−200 mJ cm^{-2} (308 nm). Slight focusing of the 308 nm beam was used to achieve the desired intensities (see below). The low repetition rate allowed for replacement of the photolyzed gas sample between laser pulses, thereby limiting the build-up of reaction products. Emission from I* was observed using a 0.2 m monochromator to select the 1.31 μm light from the I*→I emission. A fast germanium detector (ADC 403HS) monitored the light exiting the monochromator. Fluorescence decay curves were captured and signal averaged using a digital oscilloscope (LeCroy ScopeStation LS140, 100 MHz bandwidth).

Quenching of I* by Cl_2 was examined using 248 nm photolysis, as Cl_2 has a very small absorption cross section at this wavelength. The high-frequency edge of the absorption continuum is excited by 248 nm radiation. Consequently, the absorption cross section is temperature dependent, increasing from 0.24×10^{-21} to 2.6×10^{-21} cm^2 over the temperature range from 297 to 663 K.[15] At the highest temperature, a typical photolysis laser flux of 25 mJ cm^{-2} resulted in photolysis of 0.01% of the Cl_2. To observe the quenching augmented by the presence of Cl atoms, the CF_3I/Cl_2 mixture was co-photolyzed using 308 nm pulses. The absorption cross section of Cl_2 at this wavelength is almost temperature independent, decreasing from 1.7×10^{-19} cm^2 at 297 K to 1.6×10^{-19} cm^2 at 663 K.[15] The quantum yield for dissociation at 308 nm is unity. A photolysis laser flux of 100 mJ cm^{-2} dissociates approximately 3% of the Cl_2. To differentiate the quenching by Cl atoms from that of Cl_2 and background impurities, decay curves were recorded using 248 and 308 nm photolysis, with the total pressure, gas composition, and temperature held constant. The difference in the decay rates ($\Delta\Gamma$) was related to quenching by Cl atoms. To observe well-defined differences in the decay rates, the 308 nm laser beam was adjusted to provide relatively high intensities. As the laser was positioned some 5 m away from the photolysis cell, a 1 m focal length lens was used to compensate for the beam divergence and effect a reduction in the beam cross section over the region of the cell viewed by the detector (a path length of approximately 2 cm). Measurements taken at temperatures below 500 K were conducted with the lens placed 1.6 m away from the center of the cell. For temperatures above 500 K the differences in the decay rates for 248 and 308 nm photolysis were found to be small and difficult to determine reliably. To improve this situation, the effective intensity of the 308 nm light was increased by reducing the distance between the lens and the center of the cell to 1.4 m.

To obtain the Cl quenching rate constant from these measurements, we needed to know the concentration of atoms generated by 308 nm photolysis. In principle, this could be obtained from the laser intensity and Cl_2 absorption cross section. To determine the laser intensities, we measured the pulse energies using a Scientech calorimeter, and burn patterns were used to define the beam cross-section. However, there was some uncertainty in assessing the intensity arriving at the center of the fluores-

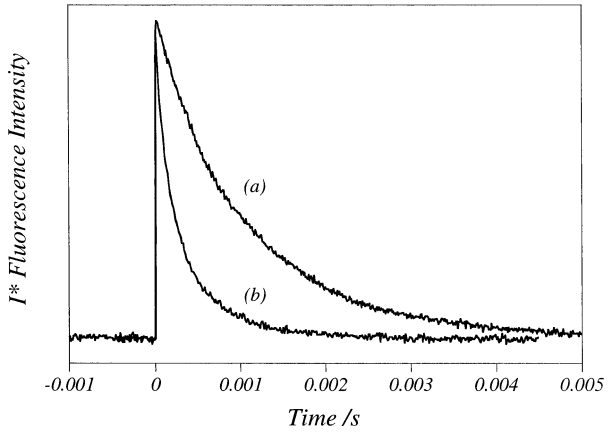

Figure 2. I* Fluorescence decay curves recorded using 248 nm (trace a) and 308 nm (trace b) photolysis at room temperature. The gas mixture consisted of 0.04 Torr of Cl_2, 0.5 Torr of CF_3I, and 11 Torr of He. These curves illustrate the dramatic increase in the fluorescence decay rate that occurs when 308 nm light generates Cl atoms.

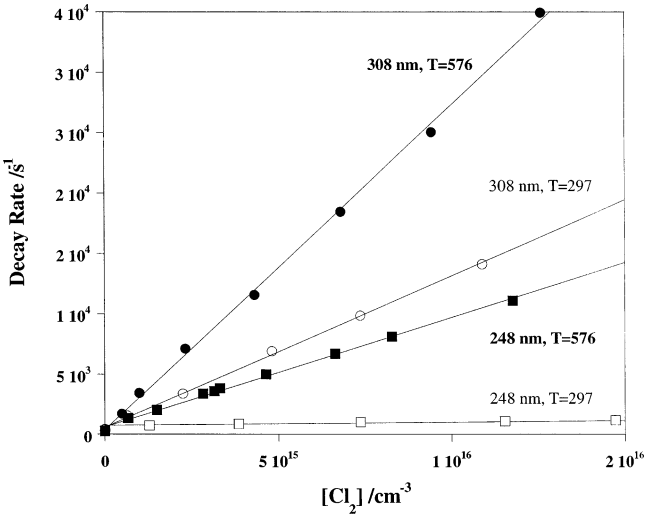

Figure 3. Stern-Volmer plots for the quenching of I* by Cl_2 and Cl atoms. The open and filled symbols correspond to $T = 297$ and 576 K, respectively. Squares and circles are used to represent 248 and 308 nm photolysis data.

cence cell, as we did not have a means to validate the calibration of the power meter. Consequently, the dissociation fraction was determined from the room temperature data using a simple kinetic model that incorporated previously determined rate constants for the key reactions (described in the following section). As the Cl_2 absorption cross section at 308 nm is effectively temperature independent over the range of interest,[15] determinations of the dissociation fraction made at room temperature were assumed to be valid for quenching measurements carried out at elevated temperatures.

Results and Analysis

Figure 2 shows typical examples of the decay curves obtained in this study. Curves a and b correspond to photolysis of the same CF_3I/Cl_2 mixture at 248 and 308 nm, respectively. The dramatic change in the decay rates reflects the very efficient quenching by the Cl atoms produced by 308 nm photolysis. Fluorescence decay curves were recorded for a range of Cl_2 pressures at temperatures of 297, 369, 437, 576, and 663 K. Stern−Volmer plots (decay rate vs quenching gas number density) for the runs at 297 and 576 K are shown in Figure 3. Two data sets are shown for each temperature, corresponding to 248 and 308 nm photolysis. Effective quenching rate constants, derived from Stern−Volmer plots are presented in Table 1. Note that the difference in the effective rate constants for 248 and 308 nm photolysis decreases markedly with increasing temperature. This occurs because the 248 nm rate constant increases dramatically with temperature, whereas the 308 nm rate constant exhibits a far more modest dependence.

TABLE 1: Measured and Fitted Rate Constants[a] for the Removal of I* by Cl_2 and Cl

T/K	$k_{obs}(248)$ [b]	$k_{obs}(308)$ [b]	k_2 [c]	k_3 [d]	*F* [e]
297	0.29	13	0.055	150	0.04
369	1.3	14	0.85	150	0.04
437	2.1	16	1.6	180	0.04
576	9.1	27	8.5	180	0.06
663	75	78	75	*f*	0.06

[a] The rate constants are in units of 10^{-3} cm^{-3} s^{-1}. [b] 1σ error limits are estimated to be ±10%. This is appreciably greater than the statisical errors resulting from the fits to the decay rate data. [c] The k_2 value for $T = 297$ K was fixed at the value reported in ref 7. The 1σ errors of the fitted values ($T \geq 369$ K) are estimated to be ±15%. [d] 1σ error limits are estimated to be ±20% [e] Fraction of Cl_2 dissociated by the 308 nm light. [f] Rate constant could not be determined because of the dominance of the Cl_2+I* quenching process.

We examined three plausible interpretations of the temperature dependence of the rate constant measured using 248 nm photolysis. In addition to the obvious interpretation (this is the temperature dependence of the rate constant for the removal of I* by Cl_2), we considered the possibility that Cl atoms were being produced by thermal dissociation of Cl_2 and/or that the effective rate constant for the dark reaction between CF_3I and Cl_2 that leads to ICl formation is strongly temperature dependent.

The standard statistical mechanics expression for the equilibrium constant was used to predict the fraction of Cl_2 that would be thermally dissociated at the highest temperatures used in this study. This calculation indicated that the number density of Cl atoms in 1 Torr of Cl_2 was 7×10^{10} cm^{-3} at 660 K. This dissociation fraction is so small that it makes a negligible contribution to the I* quenching kinetics. To test for interference from dark reactions, we varied the residence time of the gas mixture in the photolysis cell. Throttling of the pump was used to change the residence time by a factor of 4. The change in the residence time was estimated from the change in the reagent flow rates needed to maintain a constant pressure in the cell. Even at the highest temperatures, we were unable to detect any systematic dependence of the quenching rate constant on the residence time. Based on these observations and the statistical mechanics calculations, we conclude that the effect of temperature on the 248 nm measurements can be traced to the I* + Cl_2 kinetics.

A kinetic model was used to extract the Cl_2 dissociation fraction and elementary rate constants from the observed rate constants. The photochemistry of CF_3I/Cl_2 mixtures has been discussed by Hall et al.[6] and Burrows.[4] Removal of I* by Cl_2 can occur by a physical process

$$I^* + Cl_2 \rightarrow I + Cl_2 \quad (1)$$

or via the reaction

$$I^* + Cl_2 \rightarrow ICl + Cl(^2P) \quad (2)$$

In the following, the rate constants k_1 and k_2 refer to these specific channels. The distinction is kinetically significant as reaction 2 generates products that are both efficient quenchers of I*. The key reactions for the CF_3I/Cl_2 photolysis system and

TABLE 2: Reaction Set Used to Model the Room Temperature Kinetics of the CF_3I/Cl_2 Photolysis Experiments

reacn		rate constant (298 K)/cm^3 s^{-1}	ref
(1)	$I^* + Cl_2 \rightarrow I + Cl_2$	1.5×10^{-14}	4
(2)	$I^* + Cl_2 \rightarrow ICl + Cl(^2P)$	5.5×10^{-15}	7
(3)	$I^* + Cl \rightarrow I + Cl(^2P)$	1.5×10^{-11}	
(4)	$I^* + ICl \rightarrow I + ICl$	2.3×10^{-11}	7
(5)	$Cl + ICl \rightarrow Cl_2 + I$	8.0×10^{-12}	20

their room-temperature rate constants are listed in Table 2. To simulate the I* decay curves, the rate equations for this system of reactions were solved by numerical integration. Effective decay rates were obtained by fitting single-exponential decay expressions to the simulated [I*] curves. Stern−Volmer plots, constructed from the synthetic decay rates, were used to define effective rate constants.

Burrows[4] noted that the I* quenching rate constant measured using 248 nm photolysis was dependent on the intensity of the photolysis pulse. This dependence was a consequence of reaction 2. Although the reported room-temperature value for $k_1 + k_2$ is $\leq 2.0 \times 10^{-14}$ cm^3 s^{-1}, we observed an effective rate constant for I* removal of 2.9×10^{-14} cm^3 s^{-1}. Kinetic modeling of this result yielded an initial concentration for I* of approximately 1.5×10^{14} cm^{-3}, in good agreement with the concentration expected on the basis of the photolysis laser power of 25 mJ cm^{-2}. To model the room-temperature rate constant obtained using 308 nm photolysis we held all of the rate constants at the values given in Table 2 and varied the assumed laser intensity until the simulations yielded the observed quenching rate constant. The initial concentrations of I* and Cl were calculated from the temperature-dependent absorption cross-sections.[15,16] The most important parameter obtained from this procedure was the Cl_2 dissociation fraction. This was found to be 0.04 and 0.06 with the lens positioned 1.6 and 1.4 m from the center of the photolysis cell, respectively.

Care was taken to ensure that the photolysis laser intensity was held constant throughout each series of runs. As the temperature dependencies of the rate constants listed in Table 2 are unknown, we were constrained to guess which rate constants would have the most pronounced temperature dependencies. We assumed that the physical energy transfer processes would not be subject to significant energy barriers and would therefore exhibit rather modest temperature dependencies (for example, Deakin and Husain[17] found that the I* quenching rate constant for several collision partners showed only small variations over the temperature range from 180 to 410 K). In the first model described below, we assumed that the temperature dependencies observed in our experiments were a consequence of variations in the rate constants for the reactions $I^* + Cl_2 \rightarrow ICl + Cl(^2P)$ and $I^* + Cl \rightarrow I + Cl(^2P)$.

The elevated temperature data was analyzed by iteratively fitting the 248 and 308 nm results. In the first cycle, the rate constant for $I^* + Cl_2 \rightarrow ICl + Cl(^2P)$ (k_2) was varied to reproduce the 248 nm effective rate constant. By including the appropriate Cl_2 dissociation fraction, the model was then used to predict the rate constant for 308 nm photolysis. For the $T = 369$ K data, this procedure converged in a single step. Simply increasing k_2 to 8.5×10^{-14} cm^3 s^{-1} gave a good fit to the 248 and 308 nm data. For the $T = 437$ and 576 K data, increasing k_2 alone was not quite enough to account for the 308 nm rate constant. Good agreement was obtained by increasing k_3 to 1.8×10^{-11} cm^3 s^{-1} for both data sets (this change had a negligible effect on the simulations of the 248 nm data). Analysis of the

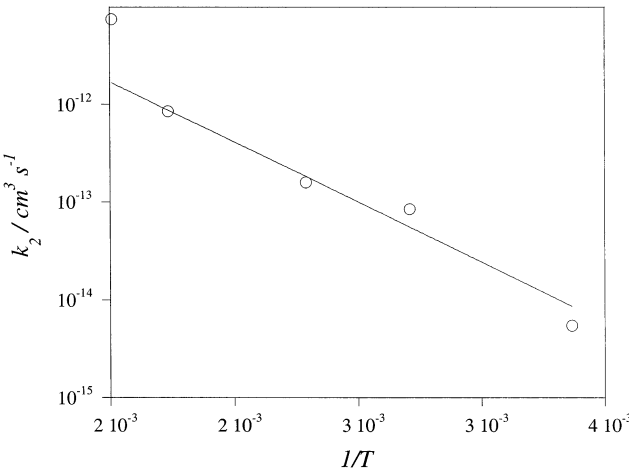

Figure 4. Arrhenius plot for the $I^* + Cl_2$ rate constant as a function of temperature. Note that the data point at 663 K was not used to generate the fitted line.

$T = 663$ K data indicated that k_2 had increased dramatically in going from 576 to 663 K. We were unable to extract a meaningful value for k_3 at 663 K as the error ranges for the 248 and 308 nm rate constants were overlapped.

Unfortunately, the kinetic model could not be used to determine whether the temperature dependence of the Cl_2 quenching rate constant was due to the chemical channel, the physical channel, or some combination of the two. In a second series of kinetics simulations, we found that the data could be satisfactorily modeled by assuming that the k_1 rate constant ($I^* + Cl_2 \rightarrow I + Cl_2$) carried the temperature dependence. With k_2 fixed at a temperature independent value of 5.5×10^{-14} cm^3 s^{-1}, the model yielded values for k_1 that were very close to the 248 nm rate constants given in Table 1. This model still required an increase in k_3 to 1.8×10^{-11} cm^3 s^{-1} for the 437 and 576 K data.

Rate constants extracted from the first kinetic model are listed in Table 1. Consistent with other physical I* quenching processes, we found that the rate constant for $I^* + Cl$ is almost temperature independent. Conversely, the rate constant for removal of I* by Cl_2 has a strong temperature dependence. The fitted k_2 values for $T \leq 576$ K are well represented by the Arrhenius expression

$$k_2 = A \exp\left(\frac{-E_{act}}{RT}\right) \qquad \text{(E1)}$$

Figure 4 shows a plot of $\ln(k_2)$ vs $1/T$. The solid line in this plot was obtained from a direct fit of eq E1 to the $T \leq 576$ K data. The $T = 663$ K data point was omitted from the fit as the large deviation from the curve defined by the lower temperature data suggests that additional quenching channels may become important above 600 K. The line in Figure 4 represents the Arrhenius parameters $A = 1.2 \times 10^{-10}$ cm^3 s^{-1} and $E_{act} = 24$ kJ mol^{-1} (inclusion of the 663 K data yields less reasonable preexponential factor of $A = 2.1 \times 10^{-7}$ cm^3 s^{-1} and $E_{act} = 57$ kJ mol^{-1}).

Theoretical Model of I* + Cl Quenching

The calculations of Yabushita[14] indicate that a curve crossing between the $I^* + Cl$ 0^+(IV) and $I + Cl^*$ 0^+(III) potential energy curves will provide the most facile channel for $I^* + Cl$ quenching. This crossing is located at an interatomic separation of $R_x = 2.85$ Å, at an energy $V(R_x) = 850$ cm^{-1} below the $I^* + Cl$ dissociation asymptote. The interaction energy at the

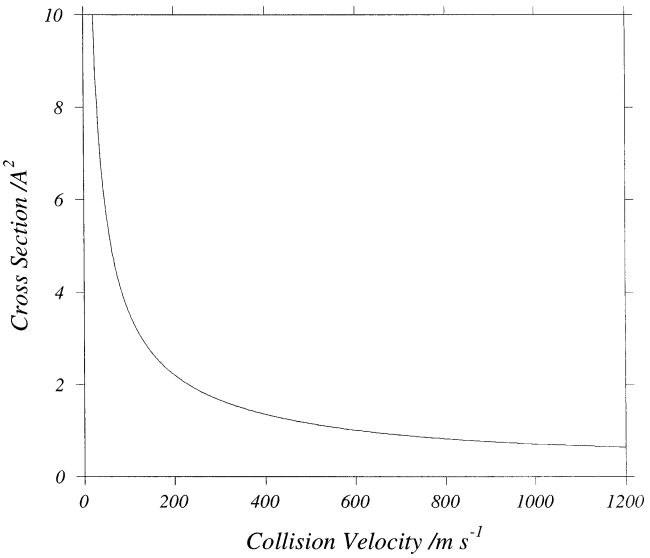

Figure 5. Calculated cross section for I* + Cl quenching as a function of the collision velocity. This calculation is for collisions that begin on the 0^+(IV) potential energy curve. See text for details.

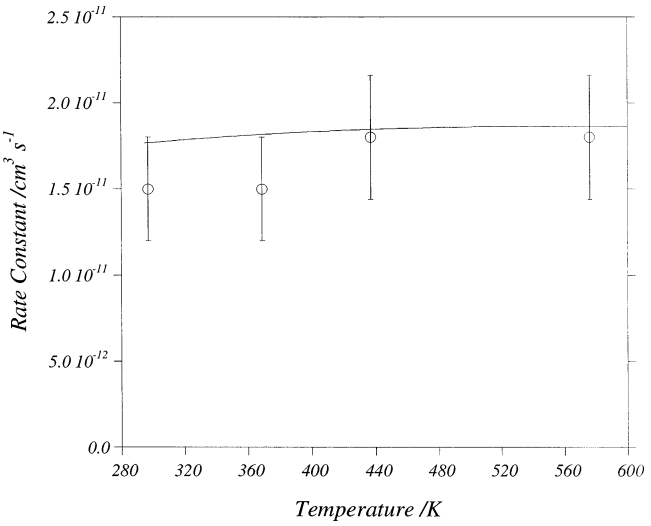

Figure 6. Comparison of the calculated rate constant for I* + Cl quenching with the measured values over the temperature range 290−600 K. The error bars for the measured rate constants are estimated to be ±20%.

crossing point is $V_{12} = 245$ cm^{-1}, and the difference in the slopes of the potential curves is $\Delta F = 7791$ cm^{-1}.

We have used Chang and Pritchard's[18] formulation of the Landau−Zener model to predict the quenching rate constant from the curve crossing parameters. This model was chosen as it includes the effect of the centrifugal barrier for nonzero impact parameters. The model is expressed in terms of the following variables: v is the relative velocity of the collision pair at infinite separation, which defines the collision energy, $E = \mu v^2/2$, where μ is the reduced mass. The Landau−Zener parameter is defined by $v_0 = 2\pi V_{12}^2/\hbar|\Delta F|$, v_x is the velocity at the crossing point, and v_x* is a reduced variable given by $v_x^* = v_x/v_0$. A reduced interaction term is defined by $V_x^* = 2V(R_x)/\mu v_0^2$. For a given collision energy the maximum impact parameter that will permit the collision pair to pass over the centrifugal barrier is given by b_{max}'. Note that b_{max}' depends on the functional form of the long-range potential for I* + Cl. In the following calculations we have assumed an R^{-6} dependence (the same form was adopted by Chang and Pritchard[18] in their analysis of I + Br → I + Br* collisions).

In terms of the parameters defined above, the quenching cross section for collisions occurring with velocity v is given by

$$\sigma(v) = 4F(v_x^*, b_{max}')\left(1 + \frac{V_x^*}{v_x^{*2}}\right)^{-1} \pi R_x^2 \qquad \text{(E2)}$$

with

$$F(v_x^*, b_{max}') = \int_1^{x_c} \frac{1}{x^3} \exp\left(-\frac{x}{v_x^*}\right)\left[1 - \exp\left(-\frac{x}{v_x^*}\right)\right] dx \qquad \text{(E3)}$$

and

$$x_c = \left(1 - \left(\frac{b_{max}'}{R_x}\right)^2 \frac{E}{E - V(R_x)}\right)^{-1/2} \qquad \text{(E4)}$$

The cross section for I* + Cl, calculated as a function of the velocity, is shown in Figure 5. At low collision velocities, the cross section becomes large due to the ability of the long-range forces to pull the slow moving collision partners toward one another. The decrease in the cross section at high collision velocities, for energies where the long-range attractive forces are unimportant, results from the rapid passage through the curve crossing region which reduces the transition probability. The thermal rate constant can be calculated from the velocity dependent cross section using the standard expression

$$k'(T) = \int_0^\infty v g(v) \sigma(v)\, dv \qquad \text{(E5)}$$

where $g(v)$ is the thermal velocity distribution function. In using eq E5 to compute the rate constant, we weight the result by a statistical factor that accounts for the fact that many collisions will not sample the 0^+(IV) state. The states $\Omega = 2, 1, 1, 0^+$, and 0^- correlate with I* + Cl. As the states with $\Omega > 0$ are 2-fold degenerate, this means that the collision partners may approach along any one of eight available potential energy curves. Hence, the rate constants calculated from eq E5 must be weighted by a factor of 1/8 to obtain results that may be directly compared with experiment. The smooth curve in Figure 6 shows a plot of the calculated rate constant as a function of temperature. The level of agreement with the experimental results is satisfactory, given the simplicity of the model.

Discussion

Our room-temperature measurements of the quenching of I* by Cl and Cl_2 yielded results that were consistent with the studies of Burrows,[4] De Juan and Smith,[5] and Lilenfeld et al.[7] Consequently, we used the results from the earlier investigations in the analysis of the present data. Hall et al.[6] reported rate constants of 2×10^{-10} cm^3 s^{-1} and $<8 \times 10^{-15}$ cm^3 s^{-1} for quenching by Cl and Cl_2, respectively. The former is far larger than the results of Burrows[4] and De Juan and Smith,[5] whereas the latter is much smaller than previous estimates for I* + Cl_2.[4,7] Small rate constants are notoriously difficult to characterize. Quenching and reactions that involve impurities can easily result in measured rate constants that are much larger that the true values. Hence, it is likely that the small value for the I* + Cl_2 quenching rate constant reported by Hall et al.[6] is the most reliable. Analysis of the data obtained in the present study yields a value for $k_1 + k_2$ that is a factor of 2.5 greater than the quenching rate constant of Hall et al.[6] This discrepancy may have been caused by the presence of impurity O_2 in our Cl_2 sample. Quenching of I* by O_2 is rapid ($k(298) = 2.5 \times 10^{-11}$ cm^3 s^{-1})[17] so the presence of 0.04% contamination could

account for the difference. Because of the dramatic increase in the Cl_2 quenching rate constant with temperature, the possible influence of quenching by impurities becomes much less significant for $T > 350$ K. For example, consider the influence of 0.04% O_2 contamination on the results for $T = 369$ K. The O_2 quenching rate constant is 2.7×10^{-11} cm^3 s^{-1} at this temperature,[17] resulting in an overestimation of the 8.5×10^{-14} cm^3 s^{-1} I* + Cl_2 rate constant of 10%. This is comparable to the measurement error. In our kinetic models, we have used the effective rate constant for reaction 1 (Table 2) which implicitly corrects for the possible influence of quenching by impurities.

Hall et al.[6] examined the role of Cl quenching by varying the intensity of their photolysis laser. Their study was limited in the sense that they used only one photolysis wavelength (266 nm). Using 248 and 308 nm photolysis allows for a large variation of the initial Cl concentration while the initial I* concentration is held nearly constant. Attempts to interpret our data using the rate constants of Hall et al.[6] were not successful. To model the 248 nm data, we needed to reduce the initial I* concentration to 5×10^{13} cm^{-3}, which is about a factor of 3 lower than we would estimate from the laser intensity and CF_3I density. Modeling of the 308 nm photolysis data yielded a Cl_2 dissociation fraction of just 0.06%, which was inconsistent with the laser intensity used. Similarly, the data from Burrows[4] study does not support the higher Cl quenching rate constant. Burrows examined Cl quenching under conditions where 1.8% of the Cl_2 was dissociated. He observed an effective rate constant of 4.3×10^{-13} cm^3 s^{-1} (see Figure 7 of ref 4). Using Hall et al.'s[6] value for k_3, the effective rate constant is predicted to be 7.2×10^{-12} cm^3 s^{-1}. These considerations were the basis for adopting the values for the rate constants for reactions 1 and 3 that are given in Table 2.

Kinetic modeling led to the conclusion that the rate constant for I* + Cl quenching is almost temperature independent over the range examined. This result did not depend on assumptions made about the mechanism of quenching by Cl_2. A weak temperature dependence for I* + Cl was consistent with the trends expected for physical quenching. Furthermore, a theoretical model that incorporated calculated properties of excited states of ICl gave a near quantitative prediction of the rate constant over the 300−600 K range.

Previous investigators[6,5,7] have noted that quenching of I* by Cl_2 at room temperature is anomalously slow when compared with quenching by Br_2 (5.5×10^{-11} cm^3 s^{-1}), ICl(1.5×10^{-11} cm^3 s^{-1}), and I_2 (3.5×10^{-11} cm^3 s^{-1}). Quenching by Br_2 occurs via the reaction I* + Br_2 → IBr + Br*, whereas collisions between I* and I_2 result in electronic to vibrational energy transfer, with $I_2(X)$ levels around $v = 40$ being populated. The rate constant seems unusually large for this E−V process, so the mechanism is thought to involve transient formation of the chemically bound I_3 intermediate. In their discussion of the I* + Br_2 reaction, Wiesenfeld and Wolk[19] draw attention to the fact that there will be a substantial barrier to reaction for the collinear approach geometry. Orbital overlap considerations favor the side-on approach of the I*, with insertion into the Br−Br bond followed by dissociation to Br* + IBr. The large room-temperature rate constant indicates that there is little or no barrier for this channel. Hall et al.[6] speculated that the slow quenching of I* by Cl_2 may indicate that there is a significant barrier for the reaction, even for the side-on approach. They suggested that the smaller interatomic distance of Cl_2 might be less favorable for the insertion reaction. The present results indicate that the height of the barrier to the I* + Cl_2 reaction is approximately 24 kJ mol^{-1}. Although it seems reasonable that the reactive channel is responsible for the temperature dependence of the Cl_2 quenching rate constant, the present experiments are not conclusive on this point as they are not able to reveal the identity of the products. In future work, it will be of interest to monitor the formation of ICl.

With regard to the NCl(a)/I* laser system, the findings of this study indicate that problems associated with Cl atom quenching will not become more severe at the high temperatures that are predicted for subsonic laser devices. That being said, we see that Cl is an effective quencher of I* over the temperature range of interest, and quenching by Cl_2 becomes important at the high end of the range. Hence, minimization of the concentrations of Cl and Cl_2 in the active gain medium should be one of the criteria used in selecting the operating conditions.

Acknowledgment. We are grateful to the Air Force Office of Scientific Research for support of this work through Grant AFOSR F49620-02-1-0331.

References and Notes

(1) Perram, G. P. *Int. J. Chem. Kinet.* **1995**, *27*, 817.
(2) Deakin, J. J.; Husain, D. *J. Photochem.* **1972**, *1*, 353.
(3) Hofmann, H.; Leone, S. R. *J. Chem. Phys.* **1978**, *69*, 641.
(4) Burrows, M. D. *J. Chem. Phys.* **1984**, *81*, 3546.
(5) De Juan, J.; Smith, I. W. M. *J. Chem. Soc., Faraday Trans. 2* **1985**, *81*, 1695.
(6) Hall, G. E.; Arepalli, S.; Houston, P. L.; Wiesenfeld, J. R. *J. Chem. Phys.* **1985**, *82*, 2590.
(7) Lilenfeld, H. V.; Whitefield, P. D.; Bradburn, G. R. *J. Phys. Chem* **1984**, *88*, 6158.
(8) Herbelin, J. M.; Henshaw, T. L.; Rafferty, B. D.; Anderson, B. T.; Tate, R. F.; Madden, T. J.; Manke, G. C., II.; Hager, G. D. *Chem. Phys. Lett.* **1999**, *299*, 583.
(9) Henshaw, T. L.; Manke, G. C., II.; Madden, T. J.; Berman, M. R.; Hager, G. D. *Chem. Phys. Lett.* **2000**, *325*, 537.
(10) Clyne, M. A. A.; MacRobert, A. J. *J. Chem. Soc., Faraday Trans. 2* **1983**, *79*, 283.
(11) De Vries, M. S.; Van Veen, N. J. A.; Hutchinson, M.; De Vries, A. E. *Chem. Phys.* **1980**, *51*, 159.
(12) Jung, K.-W.; Ahmadi, T. S.; El-Sayed, M. A. *J. Phys. Chem. A* **1997**, *101*, 6562.
(13) Tonokorua, K.; Matsumi, Y.; Kawasaki, M.; Kim, H. L.; Yabushita, S.; Fujimura, S.; Saito, K. *J. Chem. Phys.* **1993**, *99*, 3461.
(14) Yabushita, S. *J. Mol. Struct. (THEOCHEM)* **1999**, *461*−*462*, 523.
(15) Maric, D.; Burrows, J. P.; Meller, R.; Moortgat, G. K. *J. Photochem. Photobiol. A: Chem.* **1993**, *70*, 205.
(16) Rattigan, O. V.; Shallcross, D. E.; Cox, R. A. *J. Chem. Soc., Faraday Trans.* **1997**, *93*, 2839.
(17) Deakin, J. J.; Husain, D. *J. Chem. Soc., Faraday Trans. 2* **1972**, *68*, 1603.
(18) Chang, A. M.; Pritchard, D. E. *J. Chem. Phys.* **1979**, *70*, 4524.
(19) Wiesenfeld, J. R.; Wolk, G. L. *J. Chem. Phys.* **1978**, *69*, 1805.
(20) Clyne, M. A. A.; Cruse, H. W. *J. Chem. Soc., Faraday Trans. 2* **1972**, *68*, 1377.